NUMERICAL ANALYSIS OF ELASTIC-PLASTIC FRACTURE MECHANICS EXPERIMENTS

W.Schmitt, D. Siegele, T. Hollstein+

Two- and three-dimensional elastic-plastic finite element calculations of single edge notched tension and compact specimens are evaluated with respect to force-displacement diagram, J-Integral and, for the compact specimens, stable crack growth. For the single edge notched tension specimen the fracture mechanics parameters are calculated for different loading conditions, i.e. from bolt loading (zero angular stiffness) to friction grips (infinite angular stiffness). The results are compared with different series of elastic-plastic fracture tests. The influence of the two-dimensional models plane strain and plane stress on the global behavior of the specimens is discussed.

INTRODUCTION

The evaluation of elastic-plastic fracture mechanics material parameters - for instance the fracture toughness J_{Ic} and the critical crack tip opening displacement δ_i - and their use for an assessment of defects in a component require the knowledge of local stresses and strains in terms of J and δ as a function of the prevailing geometry and loading. Generally only forces and displacements can be measured at points far away from the crack tip. Therefore calibration experiments are needed and theoretical/numerical concepts have to be developed and checked to correlate the measured quantities with the crack tip field.

For many structural materials there exists an additional safety-margin beyond the point of initiation J_i or δ_i: Slow stable crack propagation may occur without catastrophic failure of the structure in the course of which the loads or displacements may be increased substantially above the initiation values. Most commonly, J-resistance curves are used to quantify this effect.

In the first part of this contribution the analysis of ductile fracture experiments using single edge notched tension specimens without taking into account stable crack propagation is presented. In the second part, after introducing the additional numerical tools to model the crack growth, the simulations of some side-grooved compact specimens will be discussed.

+ Fraunhofer-Institut für Werkstoffmechanik, Rosastr. 9, D-7800 Freiburg

SINGLE EDGE NOTCHED TENSION SPECIMENS

Single edge notched tension specimens of thickness B = 10,20, and 40 mm (SEN 10, SEN 20, SEN 40) - see figure 1 - have been fabricated from a 50 mm thick plate of the structural steel St E 460 (Ni-V) having a yield stress of $R_{p0.2}$ = 497 MPa and an ultimate tensile strength of R_m = 667 MPa at room temperature. The specimens were fatigue- precracked to a relative crack depth $0.2 \lesssim a/W \lesssim 0.6$. Very stiff hydraulic clamping grips with concentric flutes (instead of loading by bolts) were used to pull the specimens. The fracture mechanics tests have been conducted following the relevant ASTM standards (1,2) at room temperature; load control was used at a loading rate $\dot{K} \approx 0.8$ MPa$\sqrt{m}$/sec. During loading an integral displacement V was measured over the gage length M. Further details of the experimental arrangement can be found in reference (3).

Finite Element Calculations

The finite element calculations were performed with a modified version of the general purpose code ADINA (4). The modifications did not only include the treat of multilinear stress-strain curves but also the calculation of energy release rates and J-Integral for linear and non-linear crack problems. The crack front was modelled with collapsed elements yielding either $1/\sqrt{r}$-or $1/r$ - singularities in the strains. Two-dimensional calculations were performed using 229 nodes and 68 elements (8-noded isoparametric plane strain or plane stress) in the elastic cases, and 125 nodes and 32 elements in the elastic-plastic cases. In the three-dimensional elastic-plastic calculations a reduced modelling technique was utilised where only the part around the crack front was modelled by twenty -noded isoparametric volume elements, the remaining part of the specimen was modelled in plane stress, see figure 2. Further details of this technique can be found in reference (5).

Different boundary conditions have been used in the calculations to model a possible variation of the angular stiffness of the loading machine and the fixtures in the experiments. The conditions of constant parallel displacement of the end faces (infinite angular stiffness) and of point load or of constant stress but allowing for a rotation of the end faces simulating bolt loading (zero angular stiffness) have been considered as limiting cases.

Evaluation of Force Displacement Diagrams. For the numerical evaluations, both one experiment of a relatively thick SEN specimen with a short crack and of a thin specimen with a long crack have been chosen. The measured values of force and displacement over the length M (see figure 1) for each of these experiments are shown in figures 3 and 4 together with FE results. Experiment D 15 from reference (3) with B = 40 mm and a/W = 0.394 has been evaluated using the reduced 3D-model in figure 2.

In the first attempt all models (plane strain, plane stress and 3D) were loaded with parallel displacements of the end faces, thus simulating infinite angular stiffness of the loading device. Figure 3 shows the computed force-displacement curves (solid lines and dots) with that of the experiment (crosses). The agreement is not good, all three numerical models, even the plane stress model overestimate the force which was actually recorded in the experiment. This was very disappointing, since in references (3) and (5) excellent agreement between simulation (three-dimensional) and experiment had been found in the case of compact specimens.

In order to investigate the influence of the angular stiffness at least qualitatively, the two-dimensional calculations were repeated, but now modelling zero angular stiffness by allowing rotation of the end faces. The computed

force-displacement curves for plane strain and plane stress are given as dashed lines also in Figure 3. They lie significantly below the respective curves with infinite angular stiffness. It was concluded that a three-dimensional analysis with zero angular stiffness would again give a force-displacement curve slightly above the plane stress curve and would thus underestimate the force-displacement behavior of the specimens especially in the elastic-plastic case, and the real specimen behavior can not be modelled by one of the limiting cases with sufficient accuracy.

To investigate the influence of specimen thickness experiment D 25 with B = 10 mm and a/W = 0.602 from reference (3) was evaluated for conditions of infinite angular stiffness. Figure 4 shows that for this loading condition the numerical results are only slightly different for plane stress and 3 D. The measured forces again lie well below the calculated results.

Therefore it is concluded that the plane stress model would be sufficient to describe the force-displacement behavior of this rather thin specimen, if the loading situation could be included more accurately. In an attempt to better quantify the influence of the angular stiffness a very much simplified plane stress model of the specimen together with the loading machine was developed. For this purpose the FE mesh of the specimen was extended by a length corresponding to the distance between the fixture of the specimen and the cross head of the tension machine. A Young's modulus 10 times higher than for the SEN specimen was assigned to this part of the structure. Only parallel displacements were allowed for the end faces of the elongated structure. The resulting force-displacement curve (see figure 4) is shifted towards lower forces, and the agreement with the experimental curve is very good.

So indeed the angular stiffness is important for the force-displacement diagram; but the quality of agreement in this exercise is due to the (by chance) appropriate assessment of the loading system stiffness. More details of this study are given by Hollstein et.al. (6).

Evaluation of the J-Integral, Numerical. For two dimensional models a direct evaluation of J is possible from the original definition given by Rice (7):

$$J = \int_{\Gamma} \left(W \, dy - \vec{t} \frac{\partial \vec{u}}{\partial x} \, ds \right) \qquad (1)$$

Γ = integration path around the crack tip connecting the lower with the upper crack surface; ds = element of Γ; W = specific work of deformation; $\vec{t}$ = stress vector; $\vec{u}$ = displacement vector along the path of integration; x, y, = Cartesian coordinates.

The virtual crack extension method introduced in the finite element technique by Parks (8) allows the computation of the energy release rate and therefore J following Eq. (6) without much additional numerical effort and can easily be extended to three-dimensional situations. All results obtained so far with this version of ADINA show that the evaluation of the line integral Eq. (1) is essentially path-independent even for large plastic deformations, and the values of J agree well with the results from the virtual crack extension method.

Three-dimensional calculations show that for straight crack-fronts J varies across the thickness of the specimen and reaches a maximum in the middle. Comparison of numerical and experimental results of J for compact specimens by Schmitt and Hollstein (9) revealed that for both the single specimen technique

and the multiple specimen technique the experiment measures an average $\bar{J}$

$$\bar{J} = \frac{1}{B} \int_0^B J\,(b)\,db \qquad (2)$$

across the thickness. Therefore in the following figures for 3 D situations this average $\bar{J}$ is evaluated.

Comparison of Calculated J with Experiments

In figure 5 J-integral values measured for experiment D 15 and calculated according to different models are plotted over the load. Again as in figure 3 for the force-displacement diagrams large differences are found.

In figure 6 measured as well as calculated J-integral values are plotted against load for SEN experiment D 25. The same tendency can be seen as in figure 4; good agreement with the experimental results is found as long as no stable crack growth occurs from a calculation "2 D, plane stress, non zero angular stiffness of the loading system".

TWO DIMENSIONAL SIMULATION OF J_R-EXPERIMENTS WITH COMPACT SPECIMENS

Experimental Determination of J_R-Curves

The single specimen partial unloading compliance method was used to derive elastic plastic crack growth resistance (J_R-) curves. The main steps of this procedure are shown schematically in figure 7: determination of the crack driving parameter J-integral from the force-displacement diagram of the specimen, evaluation of the stable crack extension Δa from changes of the elastic compliance of the specimen which are determined from small partial unloadings during loading, evaluation of the resulting $J_R(\Delta a)$-curve to characterize crack initiation and crack growth by the parameters J_i and dJ_R/da. Further details of the experimental arrangement for the computer controlled testing and on line evaluation are given by Mayville and Blauel (10) and Voss and Blauel (11). The rules of the ASTM standard E 813 (2) for determination of the toughness parameter J_{Ic} were followed.

Simulation of Crack Growth in the Finite-Element Method

In order to be able to embrace stable crack growth numerically, a method developed by de Lorenzi (12) for the two-dimensional case was programmed into ADINA in slightly modified form.

In this simulation, the nodes lying on the ligament are held by stiff springs perpendicular to the crack-propagation direction, and the crack-tip nodes are displaced in the propagation direction until the corner node of the next element is reached. The two springs of the first element are then dissolved and the displacement is continued in the second element (see Fig. 8). In this manner, with a relatively coarse FE-grid even small crack length increments can be produced.

The numerical simulation of the experiment can be conducted in two ways: Either the relation between the opening displacement v and the crack propagation Δa is input as observed in the experiment and from that the load-displacement behavior of the experiment and the J_R-curve are predicted, or the

material J_R-curve is input and the load-displacement behavior as well as the v- Δa curve is predicted.

In ADINA the solution of the incremental finite element equilibrium equations yields, in general, an approximate incremental displacement vector. To improve the accuracy and to prevent the development of instabilities, equilibrium iterations are necessary, especially for problems with stable crack growth. The local load relief in the crack front area due to the crack growth causes severe problems with the convergence of the equilibrium iterations. This difficulty was solved by forcing the elastic stiffness matrix to be used for the iterations when ever crack growth occurs. In this way, significant improvements have been achieved, above all in respect of the convergence behavior of the FE-models, in the numerical methods given by Shih and De Lorenzi employed for the ADINA FE-program to deal with stable crack growth.

Results

C 25 and C 50 compact specimens with thickness, B = 25 mm and B = 50 mm, respectively, relative initial crack length a/W=0.6 and a/W=0.5 are analysed.

Fig. 9 shows for the C 50 specimens the calculated force-displacement curves for plane strain and plane stress in comparison with the experimental results. The real specimen behaviour is bounded by the curves for the two-dimensional models; in the elastic range, it is very well described by the plane-strain curve, but with the specimens in the fully plastic state the plane-stress curve takes over. This is understandable since the compliance of the side-grooved specimen during elastic deformation can be described in plane-strain, but during plastic deformation the lateral notches and the crack tip lose their constraining effect also as a consequence of the increasing radii of curvature of the crack tip with the result that the force-displacement behavior of the specimen approaches that of the plane-stress-state.

Here, the force calculated by the two-dimensional models for unit thickness have been multiplied by the net section thickness of the specimen, B_N.

Fig. 10 shows the measured and calculated force-displacement diagrams for the C 25-specimen. Here, for comparison, the computed forces for plane strain and plane stress have been multiplied by the net-section-thickness B_N and by the overall-thickness B. All computed curves follow very well the trend of the experiment. But from this exercise it cannot be concluded how the effective specimen thickness should be determined. Three-dimensional calculations would be necessary to extend the findings by Shih and de Lorenzi (13) into the elastic-plastic range.

The J-integrals for plane-strain calculated over the various integration paths (line integral) and for virtually displaced regions (method of virtual crack elongation), exhibit only slight differences as long as the integration path selected is not directly adjacent to the crack tip or even no longer embraces the crack tip. If however integration paths and displacement-regions are selected such that the distance of the path from the crack tip is not too small, even for the maximum crack extension, the J-integral remains almost path-independent. In the following, only the outermost integration path will be discussed.

Noteworthy is the finding that the values calculated using the line integral and those calculated using the method of virtual crack elongation for an equivalent integration path coincide.

Figures 11 and 12 show, for the C 50 and for the C 25 specimens respectively, the measured and the calculated J_R-curves. Since the correlation between opening displacement and crack propagation as observed in the experiments was used to control the simulation, the calculated J_R-curves for plane strain necessarily fall above those for plane stress. The experimental results lie between the plane stress and plane strain results for the C 50-specimen. In the case of the C 25-specimen, especially the experimental technique has been significantly improved. Now the experimental J_R-curve is well reproduced by the plane strain model. However, it should also be noted that the relative crack propagation with respect to the remaining ligament is larger in the case of the C 50-specimen.

A more detailed description of the experimental and numerical work is given by Voss and Blauel (11) and Siegele et al. (14).

CONCLUSIONS

The evaluation of the single edge notched tension experiments again pointed out the importance of the correct choice of the numerical model. In addition to three-dimensional effects discussed in more details in references (7) and (8) the consideration of details of the loading device was found to be necessary.

The computer simulation of J-resistance experiments using two-dimensional models produced a satisfactory measure of agreement, with differences for which rational explanations can be given; the limit cases plane strain and plane stress also provide bounds within which the real specimen behavior lies. Although the crack growth accounted for up to more than 20 % of the ligament, in the numerical methods no path-dependence was found for the J-integral calculated from the line integral. Furthermore, the J-values determined from the virtual crack extension method were in agreement with the line integral.

REFERENCES

1. ASTM E 399-81, Standard Method of Test for Plane-Strain Fracture Toughness of Metallic Materials. Annual Book of ASTM Standards, Part 10 (1981), 512-533
2. ASTM E 813-81, Standard Test for J_{Ic}, a Measure of Fracture Toughness. Annual Book of ASTM Standards, Part 10 (1981)
3. Hollstein, T., Experimentelle Untersuchungen zum Verhalten von Rissen bei elasto-plastischen Werkstoffverformungen, IWM-Bericht W1/82 (1982)
4. Bathe, K.J., ADINA, a Finite Element Program for Automatic Dynamic Incremental Nonlinear Analysis. Report 82 448-1, Massachusetts Institute of Technology, Cambridge, Mass., USA (1980)
5. Schmitt, W., Anwendung der Methode der finiten Elemente in der Bruchmechanik unter besonderer Berücksichtigung dreidimensionaler und elastisch-plastischer Probleme, IWM-Bericht W2/82 (1982)
6. Hollstein, T., Schmitt, W. and Blauel, J.G., Numerical Analysis of Ductile Fracture Experiments Using Single Edge Notched Specimens. To be published
7. Rice, J.R., A Path Independent Integral and the Approximate Analysis of Strain Concentration by Notches and Cracks. J. Appl. Mech. 35 (1968) 379-386
8. Parks, D.M., The Virtual Crack Extension Method for Nonlinear Material Behavior, Comp. Methods Appl. Mech. Eng., 12 (1977) 353-364

9. Schmitt, W., and Hollstein, T., Numerical and Experimental Evaluation of Fracture Parameters in Compact Specimens in the Elastic-Plastic Range. Transactions of the 6th Int. Conf. on SMiRT, Vol. 6, Paper G 3/4, Paris (1981)
10. Mayville, R.A., and Blauel, J.G., Die Methode der partiellen Entlastung zur Ermittlung von Rißwiderstandskurven, 12. Sitzg. d. Arbeitskreises Bruchvorgänge im DVM (1980) 383-393
11. Voss, B., and Blauel, J.G., Experimental Determination of Crack Growth Resistance Curves, presented at 4th European Conf. on Fracture, Leoben 1982, this volume preceeding paper
12. de Lorenzi, H.G., J-Integral and Crack Growth Calculations with the Finite Element Program ADINA, Methodology for Plastic Fracture. Contract RP 601-2 (1978)
13. Shih, C.F., de Lorenzi, H.G., Elastic Compliances and Stress-Intensity Factors for Side-Grooved Compact Specimens. Int. Journ. of Fracture 13 (1977), 544-548
14. Siegele, D., Schmitt, W., Stöckl, H., Numerische Ermittlung des J-Integrals unter Berücksichtigung stabilen Rißwachstums, 13. Sitzg. d. Arbeitskreises Bruchvorgänge im DVM (1981) 152-161

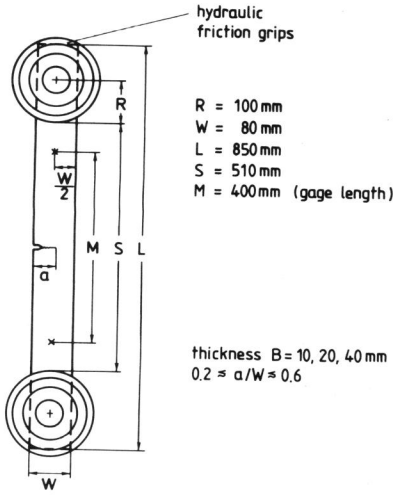

Figure 1 Single edge notched tension specimen

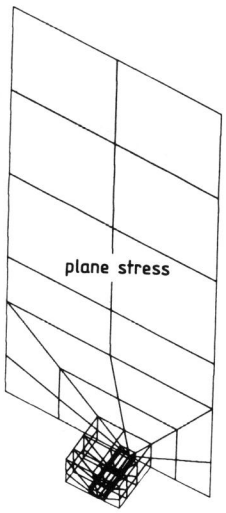

Figure 2 Reduced three dimensional FE mesh

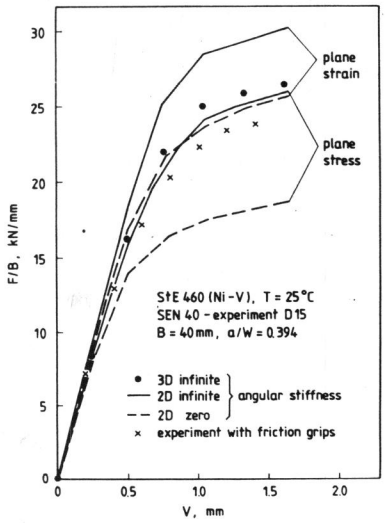

Figure 3 Force-displacement diagrams (B = 40 mm)

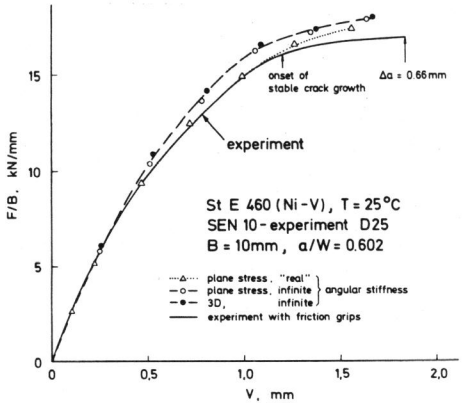

Figure 4 Force-displacement diagrams (B = 10 mm)

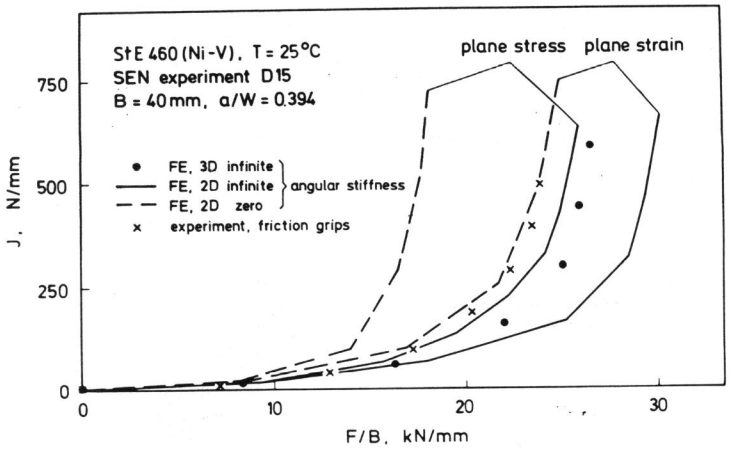

Figure 5 J-Integral as a function of force F (B = 40 mm)

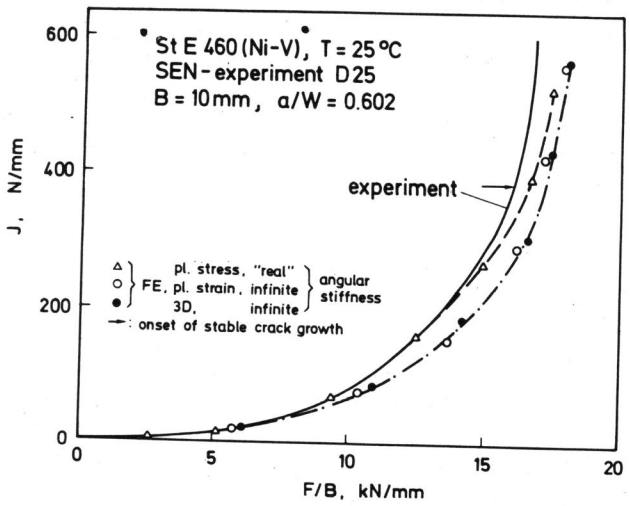

Figure 6 J-Integral as a function of force F (B = 10 mm)

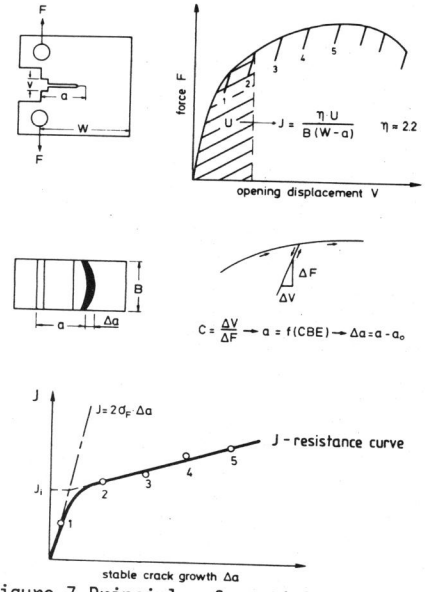

Figure 7 Principle of partial unloading compliance method

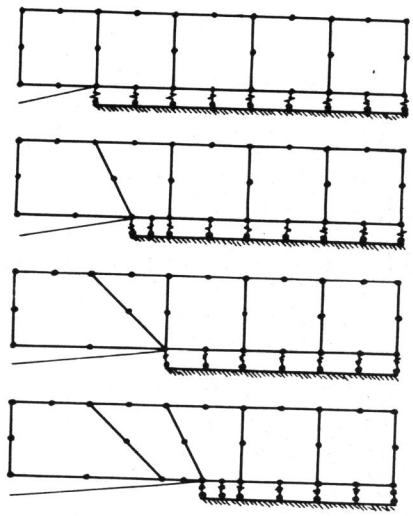

Figure 8 Numerical simulation of crack growth

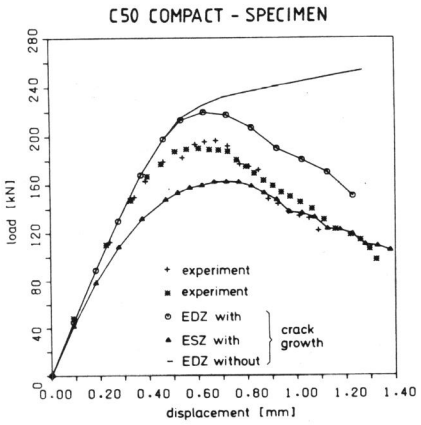

Figure 9 Force-displacement curve (B = 50 mm)

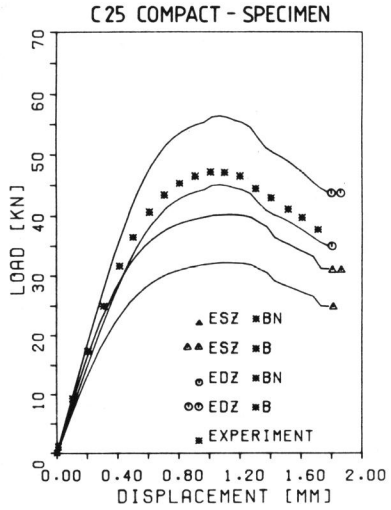

Figure 10 Force-displacement curve (B = 25 mm)

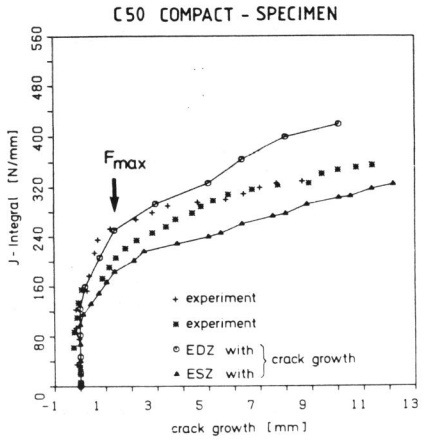

Figure 11 Crack resistance curve (B = 50 mm)

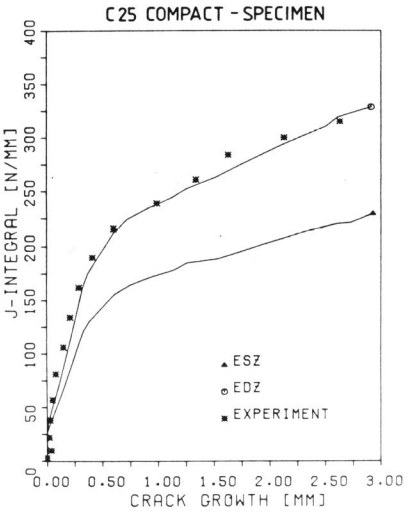

Figure 12 Crack resistance curve (B = 25 mm)